ACS APPLIED POLYMER MATERIALS

pubs.acs.org/acsapm Article

Hydrophilic Channel Volume Behavior on Proton Transport Performance of Proton Exchange Membrane in Fuel Cells

Xiangyu Huang,[⊥] Shengqiu Zhao,[⊥] Hao Liu, Rui Wang,* and Haolin Tang*

Cite This: *ACS Appl. Polym. Mater.* 2022, 4, 2423−2431 Read Online

ACCESS | Metrics & More | Article Recommendations

ABSTRACT: Inadequate water balance causes water flooding in a fuel cell, leading to performance degradation. The hydrophilic channel volume is crucial to the proton conductivity of PEM, especially under a high water concentration gradient. Herein, the volume of the hydrophilic channel was controlled and optimized through adjusting the collocation of resins with different side-chain lengths, with the length acting as a key parameter for the in-depth research on the proton conductivity performance of PEMs. Membranes with different hydrophilic channel volumes were prepared and suggested that the volume of the hydrophilic channel boosted as the increase of the length gap between the matched side chains, which would benefit to proton conductivity of membrane. This study provides guidance for the structural design of proton exchange membrane with cell-flooding resistance and efficient proton conduction at a high water concentration gradient.

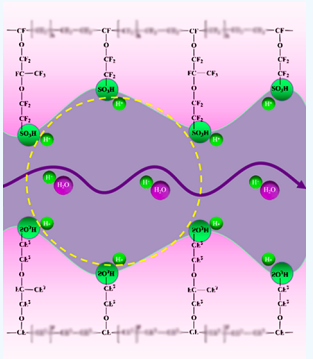

KEYWORDS: *proton exchange membrane, hydrophilic channel volume, long-side-chain, short-side-chain, proton conductivity*

1. INTRODUCTION

A fuel cell is one of the most promising energy devices, which has high energy conversion efficiency, high energy density, and zero-emission energy processes.[1−3] The proton exchange membrane (PEM) acted as a polymer electrolyte because of its superior electrochemical performance and high structural stability under hydrated condition.[4,5] Perfluorinated sulfonic acid (PFSA) is the most used PEM in PEMFC due to its high proton conductivity.[6,7]

The transport of water and proton through membrane is essential for achieving high proton conduction.[8] Benziger and colleagues have shown that when the PEM has low water activity, the rate-determining step of water transport is the diffusion of water through the PEM, but when the membrane has high water activity, the interfacial transport of water at the membrane/steam interface is the limitation of efficient water transport.[9] Commercial PFSA is composed of a tetrafluoroethylene main chain and a perfluoroalkyl ether side chain with a sulfonic acid group.[10,11] The hydrophobic perfluorinated segment of the polymer is incompatible with the hydrophilic sulfonic acid group; hence, phase separation occurs.[12,13] The PEM expands by adsorbing water, which enhances the diffusion of water and proton conductivity. Sulfonate anions and protons are dissolved in water.[14] Solvated protons are mobile, while sulfonates are fixed.[15] Xu and Gierke proved the formation of ion clusters in the Nafion membrane, which was composed of hydrated acid clusters (diameter 40−50 Å) in a hydrophobic fluorocarbon phase.[16] Sulfonate anions, protons, and adsorbed water were separated, and then a hydrophilic channel was formed in the continuous hydrophobic matrix.[17] When enough water is absorbed, the hydrophilic area permeates through the hydrophobic matrix, and the complete hydrophilic channel will be constructed; then, water and protons are transported by the hydrophilic channel.[18−21]

Long-side-chain (LSC) PFSA is the most commonly used membrane ionomer in the past few decades. Short-side-chain (SSC) PFSA has attracted widespread attention meanwhile.[22−24] Their chemical structures are different in the length of side chains, which causes a vital impact on the ion transport properties of the membrane.[25,26] The arrangement of hydrophilic proton conduction domains constitutes the morphological feature of PFSA membrane.[10,27,28] The water content of the proton exchange membrane would sharply increase when the cell operated at medium or high current density. Meanwhile, the cathode side of membrane will be flooding due to abundant production of water and electro-osmotic resistance, while the anode side of membrane would become relatively dehydrated which results in a water concentration gradient. This situation will dramatically degenerate the performance of the fuel cell and even lead to

Received: November 26, 2021
Accepted: March 9, 2022
Published: March 21, 2022

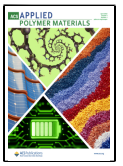

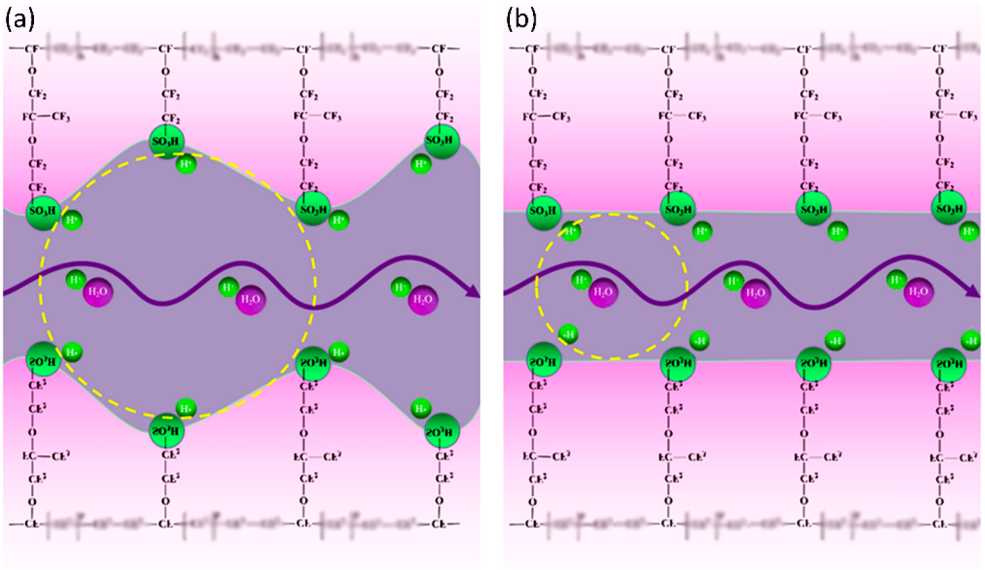

Figure 1. Schematic diagrams of proton conduction channels for (a) C2−C5 and (b) C5.

cell failure.[17,29,30] Research on a proton exchange membrane that could stably operate in a wide range of relative humidity (RH) has become an urgent issue right now.

In this paper, long-side-chain resin and short-side-chain resin were assembled to obtain samples with a collocation of different side chain lengths, and then the influence of this feature on volume was further investigated. The volume and distribution of the hydrophilic channel was evaluated through SAXS and AFM techniques. Furthermore, the effect of the mixed side chain structure on the electrochemical performance of PEM was studied by the proton conductivity test. Results showed that the volume of the hydrophilic channel would be boosted with an increase of the length gap between the matched side chains; meanwhile, the proton exchange membrane with a larger hydrophilic channel volume and connectivity shows better electrochemical performance under a high water concentration gradient.

2. MATERIALS AND METHODS

2.1. Materials and Preparation. Proton exchange membrane was prepared by blade casting method. A resin with two carbon ether side chains (D79, marked as C2) was purchased from Solvay Company. A resin with five carbon ether side chains (D2020, marked as C5) was purchased from DuPont Company. A resin with four carbon ether side chains (3M-800, marked as C4) was purchased from 3 M company. A resin with three carbon ether side chains (marked as C3) was purchased from Asahi Kasei company.

The mixed side-chain perfluorinated sulfonic acid resin was prepared by physical mixing: C2 and C5 resin solutions were mixed and stirred in a certain mass ratio (1:1, 1:2, 2:1 respectively) for 24 h. For the preparation of the membrane, the resin solution was poured onto an automatic coating machine, the height of the scraper was adjusted (by controlling the height of the scraper to control the thickness of the membrane), and a layer of coating was scraped with the resin solution. Then the coating was held at 100 °C for 3 min and thermally annealed at 150 °C for another 5 min. The samples with mass ratio of 1:1, 1:2 and 2:1 were marked as C2−C5, C2−C5 @ (1/2), and C2−C5 @ (2/1) respectively. The samples which were mixed with C2 and C5, C3 and C5, and C4 and C5 were marked as C2−C5, C3−C5, and C4−C5 respectively. C2, C3, C4 were stirred with C5 evenly for 24 h in a mixture ratio of 1:1. The membranes were prepared by a similar method.

2.2. Material Characterization. The nanostructure of the proton exchange membrane was analyzed by small-angle X-ray (SAXS), which is the most used technique to observe the nanostructure of the phase-separated polymer materials.[31,32] Before this measurement, samples were stored in a vacuum dryer for one night, and then moisturized under 80% RH for 6 h. The scattered wave vector (q) and intensity curve were measured by a Anton Paar saxsess MC2 system. The distance d was calculated using Bragg's law:[33,34]

$$d = \frac{2\pi}{q}$$

Equivalent weight (EW) of membrane refers to the mass of dry resin contained in each mole of ion group, which represents the ion exchange capacity and reflects the acid concentration in the proton exchange membrane.[35] The quantity of sulfonic acid groups per unit mass of materials is determined by an acid−base titration automatic potentiometric titrator (Metrohm titrino plus 848) through titrating the consumed H^+ with NaOH (standard solution), and then, the ion exchange equivalent could be calculated. The calculation formula is listed as follows:

$$\mathrm{EW\ (g/mol)} = \frac{W_{dry}}{V_{NaOH}C_{NaOH}}$$

Here V_{NaOH} and C_{NaOH} are the volume and concentration of NaOH consumed, respectively; W_{dry} is the membrane mass in the dry membrane state.

The surface structures of PFSA membranes have been characterized by atomic force microscopy (AFM), which has been applied to many polymer systems.[36] Percussion mode phase imaging is a relatively new AFM technology that can distinguish the hydrophilic and hydrophobic waters of PFSA membranes.[37] The membrane and microscope were placed in a specially constructed environmental chamber to control the humidity.

Proton conductivity(σ) of samples was tested by an AC impedance technique in the range from 1 MHz to 0.1 Hz, using an electrochemical workstation (Metrohm Autolab 302N). The experiments were carried out in a temperature-controlled humidity climatic chamber under variable conditions of RH (20%, 40%, 60%, 80% and 100%, respectively) at 80 °C. In addition, the sample was placed in the flooded environment for 4 h, and the conductivity was tested with the electrochemical workstation. The conductivity is calculated according to the formula as follows:

https://doi.org/10.1021/acsapm.1c01708
ACS Appl. Polym. Mater. 2022, 4, 2423−2431

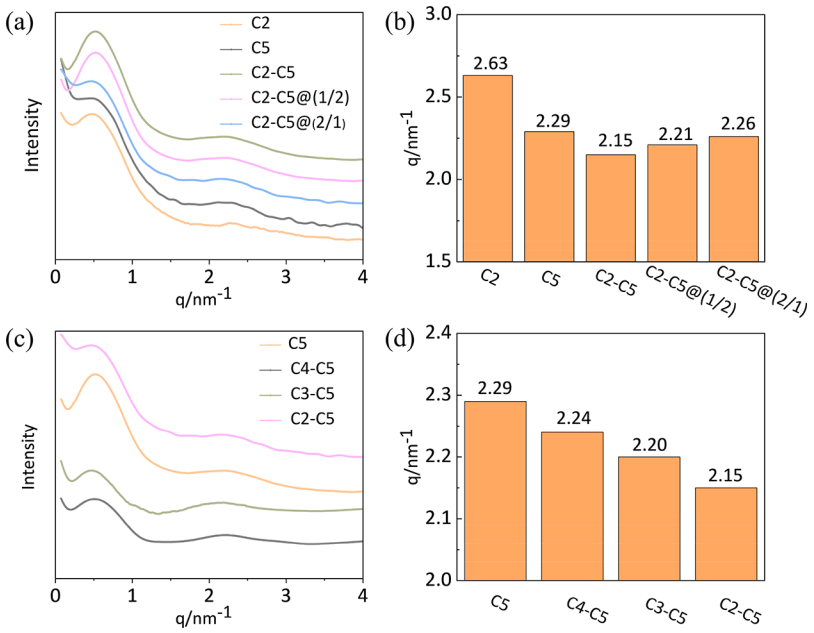

Figure 2. (a) SAXS profiles for C2, C5, C2−C5, C2−C5 @ (1/2), and C2−C5 @ (2/1) as a function of the q value at 80% RH and 298 K. (b) The q value of hydrophilic group clusters for C2, C5, C2−C5, C2−C5 @ (1/2), and C2−C5 @ (2/1). (c) SAXS profiles for C5, C4−C5, C3−C5, and C2−C5 as a function of the q value at RH80% RH and 298 K. (d) The q value of hydrophilic group clusters for C5, C4−C5, C3−C5, and C2−C5.

$$\sigma\left(\frac{S}{\text{cm}}\right) = \frac{D}{R \times L \times T}$$

Here D is the distance between the two electrodes; R is the ohmic resistance obtained from the impedance diagram; L is the width of the membrane; T is the thickness of the membrane.

The Arrhenius activation energy (E_a) is calculated by linear regression analysis of temperature-dependent conductivity curves, which is obtained according to the Arrhenius formula as follows:

$$\sigma\left(\frac{S}{\text{cm}}\right) = A \exp\left(\frac{-E_a}{R \times T}\right)$$

Here σ (S/cm), A (S/cm), R (8.314 J/K/mol), and T (K) are proton conductivity, pre-exponential factor, molar gas constant, and Kelvin temperature, respectively.

Membrane electrode assemblies (MEAs) were prepared by the decal transfer method at 423 K, 0.2 MPa. The coated catalyst layers (0.4 mg Pt/cm^2 on cathode and 0.1 mg Pt/cm^2 on anode) were supplied by Wuhan Science and Technology New Energy Company. Then, two pieces of the coated catalyst layer with an effective area of 25 cm^2 were hot-pressed onto both sides of membrane to fabricate an MEA. Before testing the polarization curve, the fuel cell was activated at 353 K with humidified H_2/O_2 to a steady state. The partial pressure of the inlet gases was kept at 150 kPa. The hydrogen crossover of the membrane was tested by using linear sweep voltammetry by scanning from 0.1 to 0.7 V with a scan rate of 2 mV s^{-1}. The anode was supplied with hydrogen at a flow rate of 200 sccm, and the cathode was supplied with nitrogen at a flow rate of 200 sccm.

3. RESULTS

As schematically illustrated in Figure 1, protons move along the well-constructed conduction channels (core) between two $-SO_3H$ layers (shell) with the size of the channels in the range of 10−30 Å. The ionic conductivity of the PEM is largely determined by the size of the proton conduction channels.[24] Figure 1 shows that the schematic diagram of the C2−C5 sample consists of a five carbon ether side chain and a two carbon ether side chain and C5 sample with a five carbon ether side chain, respectively. The volume of hydrophilic channels formed in the sample is different due to the different compositions of the side chains. Compared with proton conductors that share similar polymer backbones but contain only long acidic groups, the proton conduction channels of the polymer with uneven side chains capped by acidic groups are therefore broadened.

3.1. SAXS Test. The microstructure of the membrane was measured by SAXS. Two peaks centered on $q \approx 2.1-2.7$ and 0.5 nm^{-1} are observed in Figure 2a, which were attributed to the hydrophilic ionomer and the hydrophobic polytetrafluoroethylene matrix, respectively. The former peak represents the size of hydrophilic groups, while the matrix peak represents the long-range correlation of the main chain PTFE layered structure.[37] D spacing could be calculated by using the q corresponding to the maximum value of the peak. The q value of the hydrophilic group would be the key research point in this part. A spherical structure was assumed when we counted the size of the ionic cluster. Hosemann, Bachli, and Marx[38,39] have pointed out that the Bragg distance corresponding to the scattering peak on the SAXS scattering curve is positively correlated with the two-dimensional average area and three-dimensional average volume of scattering points. Tsao et al.[34] had confirmed that the inter aggregate distance d is positively correlated with their radius. With the absorption of water, the water molecules will be adsorbed on the sulfonic acid group, gradually forming a hydration shell, and then the hydrophilic channel formed. The radius R of ionic cluster is positively correlated with the volume of the hydrophilic channel. Furthermore , the Bragg distance d is positively correlated with the radius R of ionic cluster, and the q value is negatively correlated with the Bragg distance d, so the volume of the hydrophilic channel is negatively correlated with q value.

As shown in parts a and b of Figure 2, the maximum q values of C2 and C5 appeared at 2.63 and 2.29 nm^{-1}, which revealed that the size of hydrophilic group clusters formed by C5 sample was larger than that formed C2 sample, and then the

https://doi.org/10.1021/acsapm.1c01708
ACS Appl. Polym. Mater. 2022, 4, 2423−2431

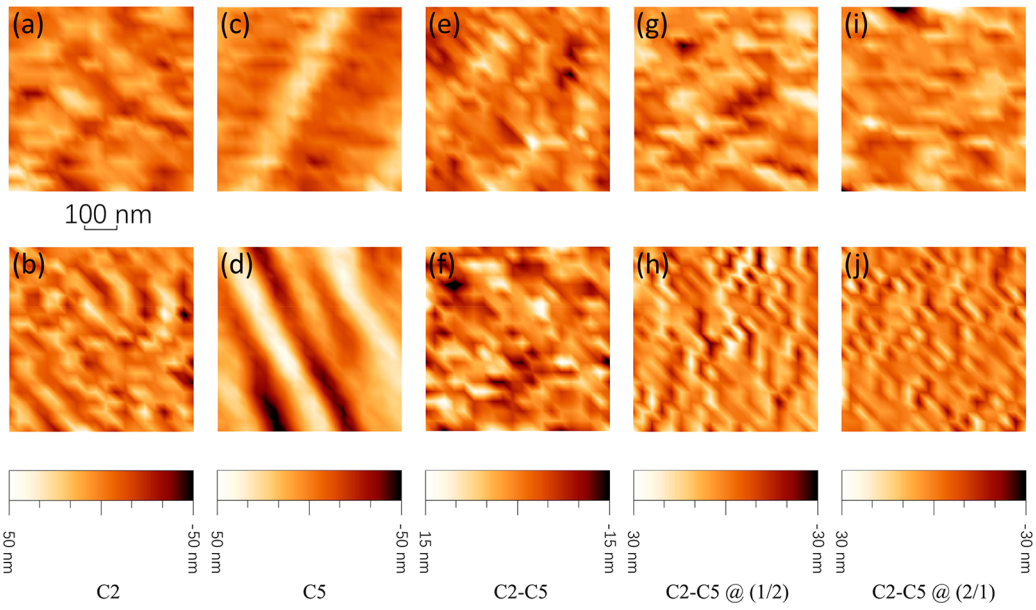

Figure 3. AFM images of samples of (a, b) C2, (c, d) C5, (e, f) C2−C5, (g, h) C2−C5 @ (1/2), and (i, j) C2−C5 @ (2/1) obtained in the tapping mode at relative humidity 20% RH (up) and relative humidity 95% RH (down) at 25 °C.

hydrophilic regional channel formed by the former was also larger than that of the latter. This conclusion was consistent with previously reported research.[40] For the proton exchange membranes with mixed side chains, the maximum q value of the ionomer peaks of C2−C5, C2−C5 @ (1/2), and C2−C5 @ (2/1) appeared at 2.18, 2.21, and 2.26 nm^{-1}, respectively (Figure 2b). The size of the hydrophilic groups formed by the C2−C5, C2−C5 @ (1/2), and C2−C5 @ (2/1) proton exchange membranes decreased successively, implying that the size of the hydrophilic channel formed thereby decreased successively. Among these samples with mixed side chains, the hydrophilic channel volume of C2−C5 was largest, which might be attributed to the situation that the mixing of long and short side chains was closest to the cross arrangement of one long and one short; hence, the hydrophilic channel was enlarged to the maximum extent. However, the mixing situation of long and short side chains was more complex between C2−C5 @ (1/2) and C2−C5 @ (2/1), and the arrangement was not optimal. The C2 sample accounted for a large proportion and there are many short side chains in the C2−C5 @ (2/1), so the hydrophilic channel formed was smaller. In conclusion, the hydrophilic channel volume of C2−C5, C2−C5 @ (1/2), and C2−C5 @ (2/1) was larger than that of C2 and C5, which proved the effectiveness of the mixed side chain strategy used herein.

As shown in Figure 2c,d, the maximum q value of the ionomer peak of C5, C4−C5, C3−C5, and C2−C5 decreased in sequence, which inferred that the size of the hydrophilic group clusters increased successively, and then the size of the hydrophilic channel formed thereby increased in order. It could be concluded that the volume of the hydrophilic channel boosts with the increase of the length gap between the matched side chains, which subsequently improved the hydrophilic channel volume of the membrane.

3.2. AFM Test. The AFM images of membranes were provided in Figure 3, where the dark region represented the hydrophilic region and the bright region represented the hydrophobic region in the PEM.[41] According to the Figure 3, the hydrophilic regions in the membrane were fuzzy and scattered, and the connectivity between each other was poor under low water content. However, the hydrophilic region in the membrane was clearly visible and the phase separation degree increased under high water content. Furthermore, the size and connectivity of the hydrophilic zones was increased. The AFM image of C2 sample showed that the dark region was small, but the connectivity between hydrophilic regions was excellent. Nevertheless, local large dark regions could be observed in the C5 sample, but the connectivity between dark regions was poor and scattered, which was the characteristic of a long side chain structure.[42−44] However, C2−C5, C2−C5 @ (1/2), and C2−C5 @ (2/1) samples show excellent size and connectivity of hydrophilic zones. Among these samples, C2−C5 had the best features and excellent connectivity of dark areas. The dark region of C2−C5 @ (1/2) was larger than that of C2−C5 @ (2/1), and the regional connectivity of the former was worse than that of the latter, which might be caused by the increase of the proportion of the two carbon ether side chain resin (C2).

3.3. EW Test. The acid equivalent of the resin decreased gradually with the increase of the proportion of C2 resin in samples with mixed side chains in Figure 4, which could be

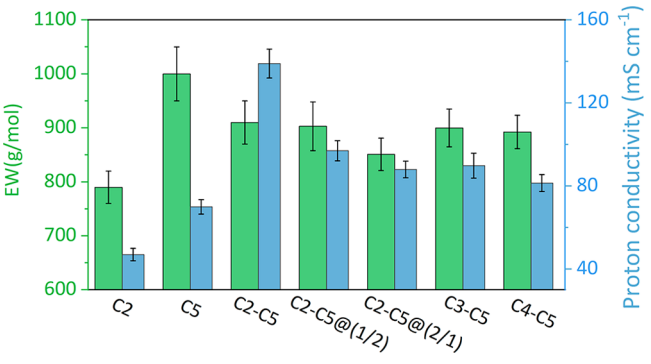

Figure 4. EW and in-plane proton conductivity of samples soaking in the water at 80 °C: C2, C5, C2−C5, C2−C5 @ (1/2), C2−C5 @ (2/1), C3−C5, and C4−C5.

https://doi.org/10.1021/acsapm.1c01708
ACS Appl. Polym. Mater. 2022, 4, 2423−2431

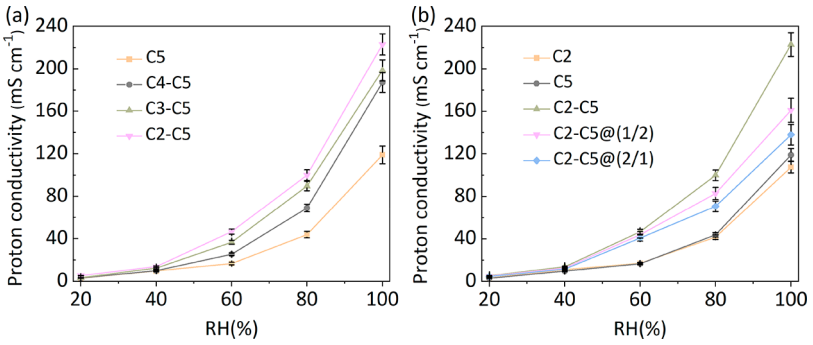

Figure 5. In-plane proton conductivity of proton exchange membrane samples: (a) C2, C5, C2−C5, C2−C5 @ (1/2), and C2−C5 @ (2/1) and (b) C5, C2−C5, C3−C5, and C4−C5 at different humidity and 80 °C.

attributed to the high content ratio of the sulfonic acid group in C2. The EW value of C2−C5 @ (2/1) was higher than that of C2−C5 @ (1/2), which indicating that C2−C5 @ (2/1) contained more sulfonic acid groups, a greater amount of water absorption and better proton conductivity in theory. The proton conductivity was tested in water to simulate the state of fuel cell under water flooding. The conductivity of C5 was higher than that of C2 in the soaking environment (Figure 4), which given rise to the larger hydrophilic channel of C5. At the same time, the proton conductivity of the mixed side chain PEMs (C2−C5, C2−C5 @ (1/2) and C2−C5 @ (2/1)) was higher than that of the single type of side chain PEMs (C2 and C5) in the soaking environment, which was attributed to the increase of hydrophilic channel volume. Overall, the proton conductivity of C2−C5 was highest, while that of C2−C5 @ (2/1) was lowest, which was ascribed to the largest hydrophilic channel formed within C2−C5.

EW values of C2−C5, C3−C5, and C4−C5 were negligible difference in Figure 4 indicating that the contents of the sulfonic acid group in the three samples were roughly equal. However, the proton conductivity in the soaking environment was apparently different, originating from the different volume of hydrophilic channels in each sample. The proton conductivity of C2−C5 was highest compared with C3−C5 and C4−C5, indicating that the volume of hydrophilic channel was largest, which was attributed to the difference between the matching side chain lengths. One could draw the conclusion that the volume of the hydrophilic channel would boost as the increase of the length gap between the matched side chains, thus having better proton conductivity performance in the waterlogged environment. This was consistent with the SAXS result.

3.4. Proton Conductivity Test. Under low humidity conditions (20%−40%), the conductivity performances of PEM with mixed side chain structures were better than those of C2 and C5 (Figure 5a), which was attributed to the structure advantage of the mixed side chain, giving PEM the characteristics of the large hydrophilic region and showing the excellent connectivity between the hydrophilic regions, so that the membrane reached the percolation threshold at low moisture content. When water content (λ) reached 1−4, the number of water molecules bound by each sulfonic acid group was low. Meanwhile the hydrated shell on the surface and the proton transport channel was not established, so that the proton transport was blocked. When λ reached at 4, a hydration shell was initially formed on the surface of sulfonic acid group, and the proton transport channel was preliminarily built successfully, reaching the percolation threshold of proton exchange membrane, which greatly increased the proton conductivity of PEM.[9,45,46] Under the condition of 60−80% RH (Figure 5a), the proton conductivity of C2−C5 was highest while the others were a little different. At this time, the water content of proton exchange membrane λ reached about 4−8, each sulfonic acid group began to form a second hydrated shell,[47] and the hydrophilic transport channels did not reach the saturated state, so the proton conductivity of five samples was high and similar. In this circumstance, the mode of proton transport is mainly the "the vehicle mechanism", which holds the point that protons move with the aid of a moving "vehicle".[48] Under high humidity conditions (100% RH), membranes with a mixed side chain structure all exhibited high proton conductivity. Meanwhile, the water content of proton exchange membrane λ was above 8, the ability of sulfonic acid group to combine water molecules reached the limit, and the excess water molecules existed in the hydrophilic channel in the form of free water. More absorbed free water could provide more carrier vehicles for hydrogen protons and continuously improved the proton conductivity of the membrane. However, when the hydrophilic channel reached the saturated state, the increased water molecules would dilute the sulfonic acid group and block the hydrophilic transport channel, thus causing degeneration of the of proton conductivity.[49] The proton conductivity of C2−C5 was excellent, which was caused by the largest hydrophilic channel. Moreover, the volume of the hydrophilic channel of C2−C5 @ (2/1) was smaller than that of C2−C5 @ (1/2) due to the large proportion of 2C resin with short side chain structure and more short side chains in C2−C5 @ (2/1). The proton conductivity of C2−C5 sample was the best while that of 5C was the worst (Figure 5b), which was related to the volume of the hydrophilic channel. The volume of the hydrophilic channel of C2−C5 was the largest, which provided great convenience for the transport of hydronium protons. The conductivity of C3−C5 and C4−C5 degenerated in sequence, which was also related to the volume of the hydrophilic channel. In conclusion, proton conductivity was positively correlated with the volume of the hydrophilic channel, which was consistent with previous SAXS and AFM results.

Proton exchange membranes were also soaked in water to measure the conductivity. The ambient temperature was 80 °C, RH was 100%, and the moisturizing time was 3 h. The conductivity of membranes in water was significantly inferior to that in the normal working condition (100% RH) in Figure 6, indicating that the occurrence of flooding phenomenon would lead to the PEM absorbing too much water, resulting in the decrease of sulfonate ion concentration. The ion channel of

https://doi.org/10.1021/acsapm.1c01708
ACS Appl. Polym. Mater. 2022, 4, 2423−2431

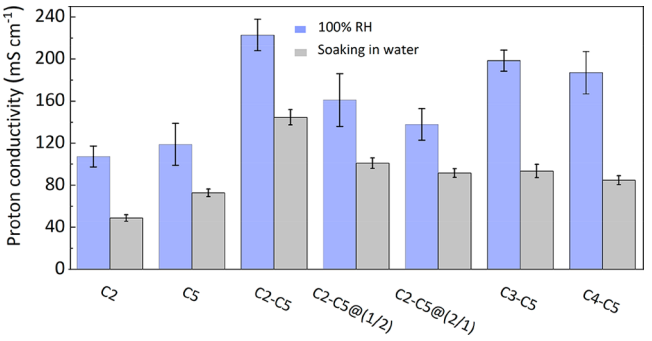

Figure 6. In-plane proton conductivity of proton exchange membrane samples C2, C5, C2−C5, C2−C5 @ (1/2), C2−C5 @ (2/1), C3−C5, and C4−C5 at 80 °C: 100% RH vs soak in the water.

C2 was narrower than C5, so the proton conductivity of C5 was slightly higher than C2. The hydrophilic channel volumes of the samples with a mixed side chain were expanded to a certain extent, which could improve the capacity to accommodate water molecules and alleviate the degeneration of the proton conductivity. Therefore, the conductivity of these samples was better than that of C2 and C5. C2−C5 exhibited better performance than C2−C5 @ (1/2) and C2−C5 @ (2/1), which was relative to the volume of hydrophilic channel. In conclusion, the proton conductivity of C2−C5, C3−C5, C4−C5, and C5 decreased in sequence, indicating that the proton conductivity of membranes soaking in water would be improved as increase of the hydrophilic channel volume. Meanwhile, by comparing the proton conductivity of samples in the water soaking environment and 100% RH, the difference in conductivity increased in the order of C2−C5, C3−C5, C4−C5, and C5, revealing that samples with large hydrophilic channel volume have better conductivity and better water-flooding resistance under high water content.

The activation energy of samples was calculated according to the Arrhenius formula at 40, 50, 60, 70, and 80 °C, and the ambient RH was 80%. Based on the logarithm of proton conductivity and the temperature scatter diagram (Figure 7a,c), the activation energy of the proton exchange membrane sample could be calculated. The activation energies of PEM were relatively low, confirming that protons conduction at low temperature environment (below 100 °C) mainly relied on the coordinated transfer of sulfonate and water molecules. Meanwhile, the activation energy of C2−C5 was lowest, amounting to 14.38 kJ/mol, while the activation energy of C2 was highest, amounting to 18.02 kJ/mol. The 2C and 5C had minimum hydrophilic channel volume and the highest activation energy while samples with mixed side chain structure generally had lower activation energy, therefore verifying the importance of hydrophilic channel volume maximization for proton conduction.

The activation energy of C2−C5 was lowest, followed by 15.12 kJ/mol for C3−C5 and 15.5 kJ/mol for C4−C5, and this situation was put down to the different collocation of side chain lengths. The volume of the hydrophilic channel would boost as the increase of the length gap between the matched side chains; hence, the activation energy of the film would be smaller. These results were generally consistent with the above analysis.

3.5. Single Cell Test. The samples were applied to PEMFC, and the single-cell was tested under different conditions. Two extreme conditions of An/Ca = 20/100% (RH) and An/Ca = 100/100% (RH) were applied to simulate the water concentration gradient phenomenon. As could be seen from Figure 8a,b, under the test conditions of An/Ca = 20/100% (RH) and An/Ca = 100/100% (RH), C2−C5 exhibited the highest output power density, and the performance of C3−C4, C4−C5 and C5 degenerated gradually due to the diminution of hydrophilic channel volume. The electrochemical impedance spectroscopy (EIS) displayed the same

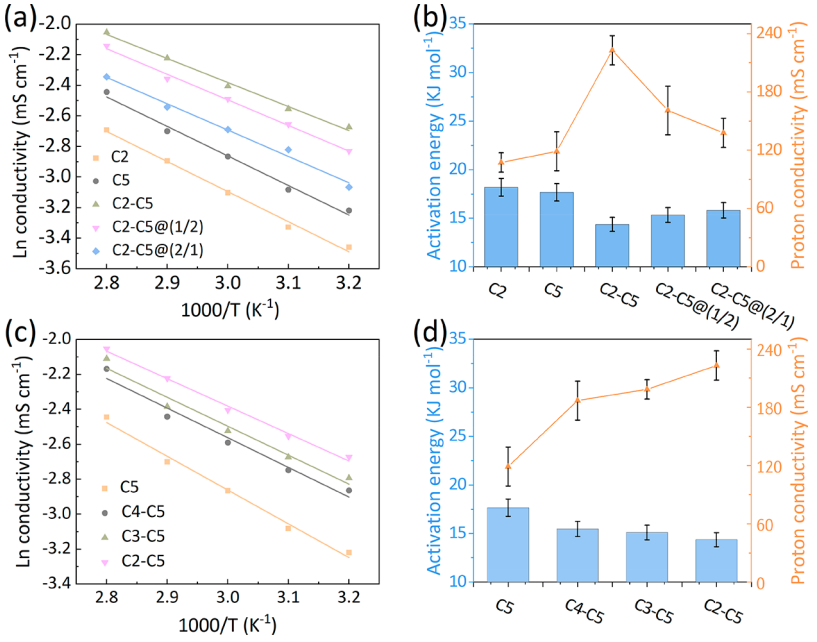

Figure 7. Temperature dependences of proton conductivity at 80% RH for (a) C2, C5, C2−C5, C2−C5 @ (1/2), and C2−C5 @ (2/1) and (c) C5, C2−C5, C3−C5, and C4−C5. Activation energy and proton conductivity (100% RH, 80 °C) of (b) C2, C5, C2−C5, C2−C5 @ (1/2), and C2−C5 @ (2/1) and (d) C5, C2−C5, C3−C5, and C4−C5.

https://doi.org/10.1021/acsapm.1c01708
ACS Appl. Polym. Mater. 2022, 4, 2423−2431

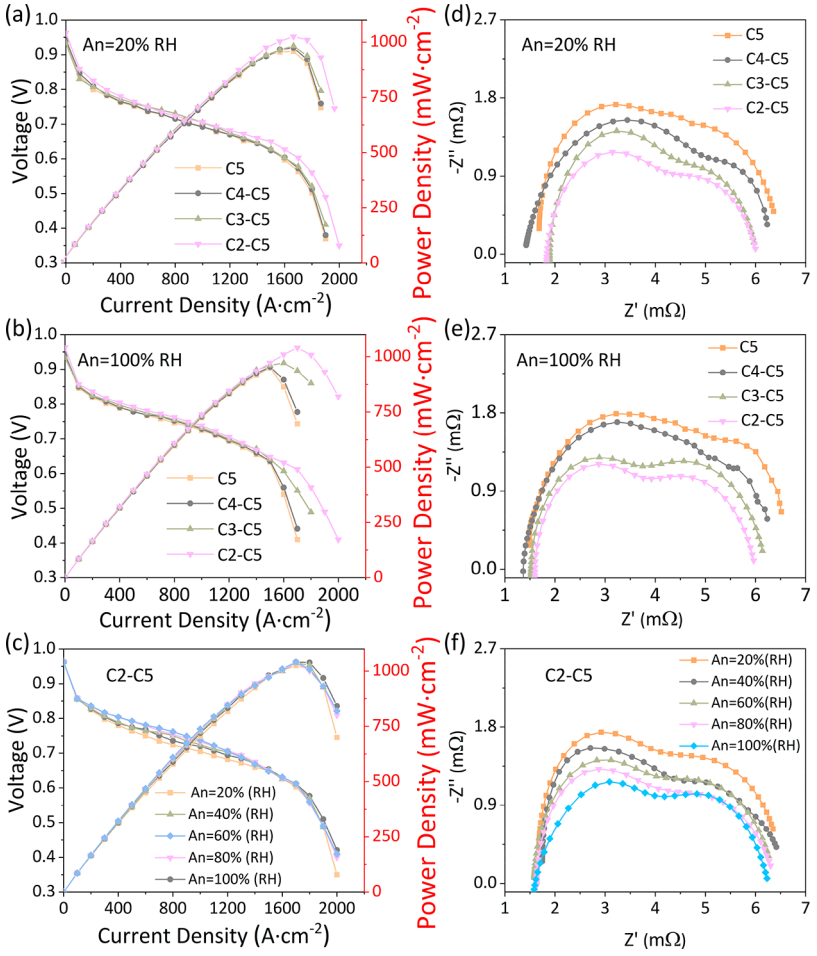

Figure 8. Polarization curves of PEMFC with test membranes at (a) An/Ca = 20/100% (RH) and (b) An/Ca = 100/100% (RH). (c) Polarization curves of PEMFC with C2−C5 from 20% to 100% (RH) in the anode. Nyquist plots of samples at (d) An/Ca = 20/100% (RH) and (e) An/Ca = 100/100% (RH) at 600 mA/cm^2. (f) Nyquist plots of C2−C5 from 20% to 100% (RH) in the anode.

tendency with the single-cell performance (Figure 8d,e). However, the samples with mixed side chains showed improved performance compared to C5, arising from the larger hydrophilic channel which could better balance the water concentration ladder difference and accommodate more water molecules. This improvement enhanced the proton conductivity and reduced ohmic loss, resulting in better cell performance. The single-cell performances exhibited similar trends to the proton conductivities of these membranes.

The cell performance of C2−C5 was excellent in the process of changing the anodic RH from 20% to 100% in Figure 8c,f. When the RH of the anode was 100%, C2−C5 showed outstanding performance at the medium and low current densies, ascribing to the fact that the domains adsorb vast water molecules provide more proton carriers for proton diffusing in vehicle mechanism.

The hydrogen crossover of the membrane was also tested with linear sweep voltammetry (LSV) by scanning from 0.1 to 0.7 V with a scan rate of 2 mV s^{-1}. The current density at 0.3 V was considered as the hydrogen crossover value of the membrane. According to Figure 9, the hydrogen crossover of each MEA increased in order of C5, C4−C5, C4−C5, and C2−C5, leading to the largest hydrogen crossover of the C2−C5 membrane, the hydrogen crossover of which reached 2.0 mA·cm^{-2} at 0.3 V. The reason for this phenomenon was probably that the hydrophilic channel volume of proton

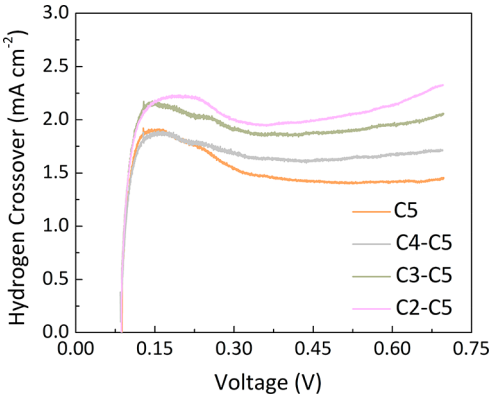

Figure 9. Hydrogen crossover results of the membranes.

exchange membrane samples with mixed side chains was large, and the volume of the hydrophilic channel would be boosted as the increase of the length gap between the matched side chains, which expanded the diffusion path of hydrogen molecules in the composite membrane and led to an increase in hydrogen crossover.

4. CONCLUSIONS

The volume and connectivity of hydrophilic channels had a crucial impact on proton transport of PEM, which was

https://doi.org/10.1021/acsapm.1c01708
ACS Appl. Polym. Mater. 2022, 4, 2423−2431

evaluated intuitively and clearly by means of SAXS, AFM, proton conductivity test and single cell test. Compared with two single side chain samples (C2 and C5), the proton exchange membrane sample with mixed side chain had a larger hydrophilic channel volume and a better hydrophilic channel connectivity, so the proton transport characteristics and proton conductivity performance of these samples were excellent. The volume of the hydrophilic channel would be boosted with the increase of the length gap between the matched side chains, so that the proton conductivity performance of the membrane was better. The hydrophilic channel volume of proton exchange membrane samples with mixed side chains was large, which had been studied by SAXS. The AFM results indicated that the hydrophilic channel volume and channel connectivity of the proton PEM with mixed side chains were excellent. The proton transport characteristics of the PEM with mixed side chains were outstanding; in particular, C2−C5 presented the best performance due to the largest volume of hydrophilic channel. The PEM with larger hydrophilic channel volume and better connectivity showed exceptional electrochemical performance under a high water concentration gradient. This study could provide guidance for the structural design of proton exchange membrane with cell-flooding resistance and efficient proton conduction at high water concentration gradients.

AUTHOR INFORMATION

Corresponding Authors

Rui Wang − *State Key Laboratory of Advanced Technology for Materials Synthesis and Processing, Wuhan University of Technology, Wuhan 430070, China; Foshan Xianhu Laboratory of the Advanced Energy Science and Technology Guangdong Laboratory, Xianhu Hydrogen Valley, Foshan 528200, China;* orcid.org/0000-0002-3616-3982; Email: rwang@whut.edu.cn

Haolin Tang − *State Key Laboratory of Advanced Technology for Materials Synthesis and Processing, Wuhan University of Technology, Wuhan 430070, China; Foshan Xianhu Laboratory of the Advanced Energy Science and Technology Guangdong Laboratory and Guangdong Hydrogen Energy Institute of WHUT, Xianhu Hydrogen Valley, Foshan 528200, China;* orcid.org/0000-0003-1041-5376; Email: thln@whut.edu.cn

Authors

Xiangyu Huang − *State Key Laboratory of Advanced Technology for Materials Synthesis and Processing, Wuhan University of Technology, Wuhan 430070, China*

Shengqiu Zhao − *State Key Laboratory of Advanced Technology for Materials Synthesis and Processing, Wuhan University of Technology, Wuhan 430070, China*

Hao Liu − *State Power Investment Corporation Hydrogen Energy Technology Development Company, Ltd., Beijing 102209, China*

Complete contact information is available at: https://pubs.acs.org/10.1021/acsapm.1c01708

Author Contributions

⊥X.H. and S.Z. contributed equally to this work.

Notes

The authors declare no competing financial interest.

ACKNOWLEDGMENTS

This work was supported by the National Natural Science Foundation of China (51976143), the National Key Research and Development Program of China (2018YFA0702001), the Key Research and Development Program of Guangdong Province (2019B090909003), the Guangdong Basic and Applied Basic Research Foundation (2020B1515120042), and the Foshan Xianhu Laboratory of the Advanced Energy Science and Technology Guangdong Laboratory (XHD2020-002).

REFERENCES

(1) Farooqui, U. R.; Ahmad, A. L.; Hamid, N. A. Graphene oxide: A promising membrane material for fuel cells. *Renew. Sust. Energy Rev.* **2018**, *82*, 714−733.

(2) Liu, Z.; Zhu, J.; Peng, C.; Wakihara, T.; Okubo, T. Continuous flow synthesis of ordered porous materials: from zeolites to metal-organic frameworks and mesoporous silica. *Reaction Chemistry & Engineering* **2019**, *4*, 1699−1720.

(3) Zhao, G. D.; Xu, X. L.; Di, Y. B.; Wang, H.; Cheng, B. W.; Shi, L.; Zhu, Y.; Zhuang, X. P.; Yin, Y. Amino acid clusters supported by cellulose nanofibers for proton exchange membranes. *J. Power Sources* **2019**, *438*, 227035.

(4) Kusoglu, A.; Weber, A. Z. New Insights into Perfluorinated Sulfonic-Acid Ionomers. *Chem. Rev.* **2017**, *117*, 987−1104.

(5) Zhao, G. D.; Xu, X. L.; Shi, L.; Cheng, B. W.; Zhuang, X. P.; Yin, Y. Biofunctionalized nanofiber hybrid proton exchange membrane based on acid-base ion-nanochannels with superior proton conductivity. *J. Power Sources* **2020**, *452*, 227839.

(6) Goh, J. T. E.; Abdul Rahim, A. R.; Masdar, M. S.; Shyuan, L. K. Enhanced Performance of Polymer Electrolyte Membranes via Modification with Ionic Liquids for Fuel Cell Applications. *Membranes (Basel)* **2021**, *11*, 395.

(7) Ran, J.; Wu, L.; He, Y. B.; Yang, Z. J.; Wang, Y. M.; Jiang, C. X.; Ge, L.; Bakangura, E.; Xu, T. W. Ion exchange membranes: New developments and applications. *J. Membr. Sci.* **2017**, *522*, 267−291.

(8) Majsztrik, P. W. Mechanical and transport properties of Nafion® for PEM fuel cells; temperature and hydration effects. *Dissertations & Theses Gradworks* **2008**, *141*, 235.

(9) Zhao, Q.; Majsztrik, P.; Benziger, J. Diffusion and interfacial transport of water in Nafion. *J. Phys. Chem. B* **2011**, *115*, 2717−2727.

(10) Kim, J. Q.; So, S.; Kim, H.-T.; Choi, S. Q. Highly Ordered Ultrathin Perfluorinated Sulfonic Acid Ionomer Membranes for Vanadium Redox Flow Battery. *ACS Energy Letters* **2021**, *6*, 184−192.

(11) Oshiba, Y.; Tomatsu, J.; Yamaguchi, T. Thin pore-filling membrane with highly packed-acid structure for high temperature and low humidity operating polymer electrolyte fuel cells. *J. Power Sources* **2018**, *394*, 67−73.

(12) Peron, J.; Mani, A.; Zhao, X.; Edwards, D.; Adachi, M.; Soboleva, T.; Shi, Z.; Xie, Z.; Navessin, T.; Holdcroft, S. Properties of Nafion® NR-211 membranes for PEMFCs. *J. Membr. Sci.* **2010**, *356*, 44−51.

(13) Zeng, Z.; Song, R.; Zhang, S.; Han, X.; Zhu, Z.; Chen, X.; Wang, L. Biomimetic N-Doped Graphene Membrane for Proton Exchange Membranes. *Nano Lett.* **2021**, *21*, 4314−4319.

(14) Yin, C.; Li, J.; Zhou, Y.; Zhang, H.; Fang, P.; He, C. Enhancement in Proton Conductivity and Thermal Stability in Nafion Membranes Induced by Incorporation of Sulfonated Carbon Nanotubes. *ACS Appl. Mater. Interfaces* **2018**, *10*, 14026−14035.

(15) Schmidt-Rohr, K.; Chen, Q. Parallel cylindrical water nanochannels in Nafion fuel-cell membranes. *Nat. Mater.* **2008**, *7*, 75−83.

(16) Gierke, T. D.; Munn, G. E.; Wilson, F. C. The morphology in nafion perfluorinated membrane products, as determined by wide- and small-angle x-ray studies. *J. Polym. Sci., Part B: Polym. Phys.* **1981**, *19*, 1687−1704.

(17) Liu, J. W.; Suraweera, N.; Keffer, D. J.; Cui, S. T.; Paddison, S. J. On the Relationship between Polymer Electrolyte Structure and Hydrated Morphology of Perfluorosulfonic Acid Membranes. *J. Phys. Chem. C* **2010**, *114*, 11279−11292.
(18) Aleksandrova, E.; Hiesgen, R.; Eberhard, D.; Friedrich, K. A.; Kaz, T.; Roduner, E. Proton conductivity study of a fuel cell membrane with nanoscale resolution. *ChemPhysChem* **2007**, *8*, 519−522.
(19) Savage, J.; Tse, Y.-L. S.; Voth, G. A. Proton Transport Mechanism of Perfluorosulfonic Acid Membranes. *J. Phys. Chem. C* **2014**, *118*, 17436−17445.
(20) Tse, Y.-L. S.; Herring, A. M.; Kim, K.; Voth, G. A. Molecular Dynamics Simulations of Proton Transport in 3M and Nafion Perfluorosulfonic Acid Membranes. *J. Phys. Chem. C* **2013**, *117*, 8079−8091.
(21) Tsui, E. M.; Cortalezzi, M. M.; Wiesner, M. R. Proton conductivity and methanol rejection by ceramic membranes derived from ferroxane and alumoxane precursors. *J. Membr. Sci.* **2007**, *306*, 8−15.
(22) Devanathan, R.; Dupuis, M. Insight from molecular modelling: does the polymer side chain length matter for transport properties of perfluorosulfonic acid membranes? *Phys. Chem. Chem. Phys.* **2012**, *14*, 11281−11295.
(23) Giancola, S.; Zaton, M.; Reyes-Carmona, A.; Dupont, M.; Donnadio, A.; Cavaliere, S.; Roziere, J.; Jones, D. J. Composite short side chain PFSA membranes for PEM water electrolysis. *J. Membr. Sci.* **2019**, *570*, 69−76.
(24) Zhang, Y.; Li, C.; Liu, X.; Yang, Z.; Dong, J.; Liu, Y.; Cai, W.; Cheng, H. Fabrication of a polymer electrolyte membrane with uneven side chains for enhancing proton conductivity. *RSC Adv.* **2016**, *6*, 79593−79601.
(25) Economou, N. J.; O'Dea, J. R.; McConnaughy, T. B.; Buratto, S. K. Morphological differences in short side chain and long side chain perfluorosulfonic acid proton exchange membranes at low and high water contents. *RSC Adv.* **2013**, *3*, 19525.
(26) Kuo, A. T.; Takeuchi, K.; Tanaka, A.; Urata, S.; Okazaki, S.; Shinoda, W. Exploring the effect of pendent side chain length on the structural and mechanical properties of hydrated perfluorosulfonic acid polymer membranes by molecular dynamics simulation. *Polymer* **2018**, *146*, 53−62.
(27) Wang, R.; Yan, X.; Wu, X.; He, G.; Du, L.; Hu, Z.; Tan, M. Modification of hydrophilic channels in Nafion membranes by DMBA: Mechanism and effects on proton conductivity. *J. Polym. Sci., Part B: Polym. Phys.* **2014**, *52*, 1107−1117.
(28) Qian, L.; Yin, C.; Liu, L.; Zhang, X.; Li, J.; Liu, Z.; Zhang, H.; Fang, P.; He, C. Magnetic aligned sulfonated carbon nanotube/Nafion composite membranes with anisotropic mechanical and proton conductive properties. *J. Mater. Sci.* **2021**, *56*, 6764−6779.
(29) Garsany, Y.; Atkinson, R. W.; Sassin, M. B.; Hjelm, R. M. E.; Gould, B. D.; Swider-Lyons, K. E. Improving PEMFC Performance Using Short-Side-Chain Low-Equivalent-Weight PFSA Ionomer in the Cathode Catalyst Layer. *J. Electrochem. Soc.* **2018**, *165*, F381−F391.
(30) Hristov, I. H.; Paddison, S. J.; Paul, R. Molecular modeling of proton transport in the short-side-chain perfluorosulfonic acid ionomer. *J. Phys. Chem. B* **2008**, *112*, 2937−2949.
(31) Martens, I.; Vamvakeros, A.; Chattot, R.; Blanco, M. V.; Rasola, M.; Pusa, J.; Jacques, S. D. M.; Bizzotto, D.; Wilkinson, D. P.; Ruffmann, B.; Heidemann, S.; Honkimäki, V.; Drnec, J. X-ray transparent proton-exchange membrane fuel cell design for in situ wide and small angle scattering tomography. *J. Power Sources* **2019**, *437*, 226906.
(32) Gebel, G.; Moore, R. B. Small-angle scattering study of short pendant chain perfuorosulfonated ionomer membranes. *Macromolecules* **2000**, *33*, 4850−4855.
(33) Fernandez Bordín, S. P.; Andrada, H. E.; Carreras, A. C.; Castellano, G. E.; Oliveira, R. G.; Galván Josa, V. M. Nafion membrane channel structure studied by small-angle X-ray scattering and Monte Carlo simulations. *Polymer* **2018**, *155*, 58−63.
(34) Tsao, C. S.; Chang, H. L.; Jeng, U. S.; Lin, J. M.; Lin, T. L. SAXS characterization of the Nafion membrane nanostructure modified by radiation cross-linkage. *Polymer* **2005**, *46*, 8430−8437.
(35) Herden, S.; Riewald, F.; Hirschfeld, J. A.; Perchthaler, M. In-plane structuring of proton exchange membrane fuel cell cathodes: Effect of ionomer equivalent weight structuring on performance and current density distribution. *J. Power Sources* **2017**, *355*, 36−43.
(36) McLean, R. S.; Doyle, M.; Sauer, B. B. High-resolution imaging of ionic domains and crystal morphology in ionomers using AFM techniques. *Macromolecules* **2000**, *33*, 6541−6550.
(37) Shin, S. H.; Nur, P. J.; Kodir, A.; Kwak, D. H.; Lee, H.; Shin, D.; Bae, B. Improving the Mechanical Durability of Short-Side-Chain Perfluorinated Polymer Electrolyte Membranes by Annealing and Physical Reinforcement. *ACS Omega* **2019**, *4*, 19153−19163.
(38) Hosemann, R.; Bagchi, S. *Direct Analysis of Diffraction by Matter*; North Holland: Amsterdam, 1962.
(39) Marx, C. L.; Caulfield, D. F.; Cooper, S. L. Morphology of ionomers. *Macromolecules* **1973**, *6*, 344−353.
(40) Min, S.; Kim, D. SAXS cluster structure and properties of sPEEK/PEI composite membranes for DMFC applications. *Solid State Ionics* **2010**, *180*, 1690−1693.
(41) Umemura, K.; Wang, T.; Hara, M.; Kuroda, R.; Uchida, O.; Nagai, M. Nanocharacterization and nanofabrication of a Nafion thin film in liquids by atomic force microscopy. *Langmuir* **2006**, *22*, 3306−3312.
(42) Gao, X. L.; Yang, Q.; Wu, H. Y.; Sun, Q. H.; Zhu, Z. Y.; Zhang, Q. G.; Zhu, A. M.; Liu, Q. L. Orderly branched anion exchange membranes bearing long flexible multication side chain for alkaline fuel cells. *J. Membr. Sci.* **2019**, *589*, 117247.
(43) Li, J.; Pan, M.; Tang, H. Understanding short-side-chain perfluorinated sulfonic acid and its application for high temperature polymer electrolyte membrane fuel cells. *RSC Adv.* **2014**, *4*, 3944−3965.
(44) Luo, X.; Holdcroft, S. Water transport through short side chain perfluorosulfonic acid ionomer membranes. *J. Membr. Sci.* **2016**, *520*, 155−165.
(45) Duan, Q.; Wang, H.; Benziger, J. Transport of liquid water through Nafion membranes. *J. Membr. Sci.* **2012**, *392*−*393*, 88−94.
(46) Motupally, S.; Becker, A. J.; Weidner, J. W. Diffusion of Water in Nafion 115 Membranes. *J. Electrochem. Soc.* **2000**, *147*, 3171.
(47) Casciola, M.; Alberti, G.; Sganappa, M.; Narducci, R. On the decay of Nafion proton conductivity at high temperature and relative humidity. *J. Power Sources* **2006**, *162*, 141−145.
(48) Wang, Z.; Tang, H.; Li, J.; Zeng, Y.; Chen, L.; Pan, M. Insight into the structural construction of a perfluorosulfonic acid membrane derived from a polymeric dispersion. *J. Power Sources* **2014**, *256*, 383−393.
(49) Benziger, J. B.; Cheah, M. J.; Klika, V.; Pavelka, M. Interfacial constraints on water and proton transport across nafion membranes. *J. Polym. Sci., Part B: Polym. Phys.* **2015**, *53*, 1580−1589.

https://doi.org/10.1021/acsapm.1c01708
ACS Appl. Polym. Mater. 2022, 4, 2423−2431